Int. J. Electrochem. Sci., 9 **(2014)** 7495 - 7505

International Journal of
ELECTROCHEMICAL
SCIENCE
www.electrochemsci.org

5,10,15,20-Tetra(4-pyridyl)-21H,23H-porphine as an effective corrosion inhibitor for N80 steel in 3.5% NaCl solution

Ambrish Singh[1,2], *Eno. E. Ebenso*[3,4,*], *M. A. Quraishi*[5], *Yuanhua Lin*[1]

[1] State Key Laboratory of Oil and Gas Reservoir Geology and Exploitation (Southwest Petroleum University), Chengdu, Sichuan 610500, China.
[2] Department of Chemistry, School of Civil Engineering, LFTS, Lovely Professional University, Phagwara, Punjab 144402, India.
[3] Department of Chemistry, School of Mathematical & Physical Sciences, North-West University(Mafikeng Campus), Private Bag X2046, Mmabatho 2735, South Africa.
[4] Material Science Innovation & Modelling (MaSIM) Research Focus Area, Faculty of Agriculture, Science and Technology, North-West University (Mafikeng Campus), Private Bag X2046, Mmabatho 2735, South Africa
[5] Department of Chemistry, Indian Institute of Technology, Banaras Hindu University, Varanasi, U.P., India.
[*]E-mail: eno.ebenso@nwu.ac.za

Received: 30 August 2014 / *Accepted:* 11 October 2014 / *Published:* 28 October 2014

The inhibition behavior of 5,10,15,20-Tetra(4-pyridyl)-21H,23H-porphine (T4PP) as an environment-benign corrosion inhibitor for N80 steel was investigated in 3.5 wt.% NaCl solution by means of potentiodynamic polarization, AC impedance, and quantum chemical calculations. The results showed that 5,10,15,20-Tetra(4-pyridyl)-21H,23H-porphine can inhibit the corrosion of N80 steel. The adsorption of T4PP on the N80 steel surface obeyed the Langmuir adsorption isotherm. The quantum chemical calculations were applied to elucidate adsorption pattern of inhibitor molecules on steel surface.

Keywords: N80 steel; Quantum calculations; Corrosion; Inhibition

1. INTRODUCTION

Use of corrosion inhibitors is the most common method used to retard corrosion of metals as no special equipments required, low cost, and easy operation. Overall, many corrosion inhibitors have some health and/or environmental problems due to their toxicity. It is highly desired that new inhibitors for N80 steel are non-toxic and environment-friendly. Use of different porphine compounds

as corrosion inhibitors is in practice nowadays as they are renewable, cheap, easily available, non toxic, which are rich in heteroatoms (N, O, S). Literature survey has concluded that compounds containing heteroatoms show good inhibition [1-8].

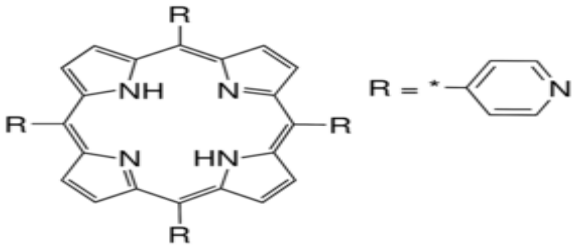

Figure 1. 5,10,15,20-Tetra(4-pyridyl)-21H,23H-porphine

2. EXPERIMENTAL

2.1. Materials and Solutions

5,10,15,20-Tetra(4-pyridyl)-21H,23H-porphine was purchased from the shop and was used in the corrosion studies. Corrosion tests were performed on a N80 steel of the following percentage composition (wt.%): C 0.31; Si 0.19; Mn 0.92; P 0.010; S 0.008; Cr 0.2; Fe balance, which were metallographically abraded according to ASTM A262, with fine grade emery papers from 600 to 1200 grade. N80 steel coupons having dimensions of 30 mm × 3 mm × 3 mm were used for the study of impedance and polarization. The test solution of 3.5% NaCl was prepared by analytical grade NaCl with double distilled water.

2.2. Electrochemical measurements

The electrochemical studies were made using an Autolab three electrode cell assembly at room temperature. The N80 steel was the working electrode, platinum electrode was used as an auxiliary electrode, and standard calomel electrode (SCE) was used as reference electrode. All electrochemical measurements were carried out using Autolab Potentiostat/Galvanostat (Model GSTAT302N) with EIS software Autolab Instruments Inc. Netherland. Autolab applications include software FRC and GPES for corrosion and EIS measurements and data fitting. Prior to the electrochemical measurement, a stabilization period of 30 minutes was allowed to attain a stable value of E_{corr}. Tafel curves were obtained by changing the electrode potential automatically from −300 to +300 mV versus corrosion potential (E_{corr}) at a sweep rate of 1 mV s^{-1}. EIS measurements were carried out in a frequency range from 100 kHz to 10 mHz under potentiodynamic conditions, with amplitude of 10 mV peak-to-peak, using AC signal at E_{corr}. The linear Tafel segments of anodic and cathodic curves were extrapolated to corrosion potential to obtain corrosion current densities (I_{corr}). The experiments were carried out when the electrochemical system was in steady state.

2.3. Scanning Electrochemical Microscopy (SECM)

Scanning electrochemical microscopy (SECM) has become one of the most powerful local techniques for corrosion research due to the wide variety of operation modes which contribute to give a great versatility to the technique [9].

The tip and substrate are part of an electrochemical cell that usually also contains other (e.g., auxiliary and reference) electrodes. The diameter of the samples used was between 30 × 3 × 3 mm. A model of scanning electrochemical microscopy CHI900C was used. The instrument was operated with a 10 μm platinum tip as the probe, an Ag/AgCl/KCl (saturated) reference electrode, and a platinum counter electrode. All potential values are referred to the Ag/AgCl/KCl (saturated) reference electrode. The measurements of line scans were generated with the tip at ~ 10 μm from the specimen surface in all the cases. The scan rate was 80 μm/step.

2.4. Quantum chemical calculations

Quantum chemical calculations were performed using density function theory (DFT) method, B3LYP with electron basis set 6-31G* (d, p) for all atoms. All the calculations were executed with Gaussian 03, E .01.The following quantum chemical indices namely energy of HOMO, LUMO, and dipole moment (μ) was determined [10].

3. RESULTS AND DISCUSSION

3.1. Electrochemical measurements

3.1.1 EIS Measurement

Impedance spectra for N80 steel in 3.5% NaCl solution in absence and presence of different concentrations of GBFE are shown in the form of Nyquist plots (Figure 2a), Bode-modulus plots (Figure 2b) and in the Theta-frequency format (Figure 2c). The impedance diagram (Nyquist) contains depressed semicircles with the center under the real axis with one capacitive loop in the high frequency (HF) zone. As usually indicated in an EIS study, the HF capacitive loop is related to the charge-transfer resistance process of the metal corrosion and the double-layer behavior, and these loops are not perfect semicircles. Such behavior is characteristic for solid electrodes and is often referred to as a frequency dispersion effect that can be imputed to nonhomogeneity and the rough-textured metal surface.

The impedance spectra for Nyquist plots were analyzed by fitting to the equivalent circuit model (Figure 2d) which was used elsewhere to describe iron / acid interface [11]. In this equivalent circuit, R_s is the solution resistance, R_{ct} is the charge transfer resistance, and CPE is a constant phase element. The double layer usually behaves as a constant-phase element (CPE) rather than as a pure capacitor. The CPE is substituted for the capacitor to fit the semicircle more accurately. The capacitance values were calculated using the equation [12]:

$$Z_{CPE} = Q^{-1}(j\omega)^{-n} \quad (1)$$

where Q is the magnitude of the CPE, j is the imaginary unit, ω is the angular frequency (ω = 2πf, the frequency in Hz), and n is the phase shift which can be used as a gauge of the heterogeneity and gives details about the degree of surface inhomogeneity (roughness). Depending on the value of n, *CPE* can represent resistance (n = 0, Q = R), capacitance (n = 1, Q = C), inductance (n = -1, Q = L) or Warburg impedance (n = 0.5, Q = W). In fact, when n is close to 1, the CPE resembles a capacitor, but the phase angle is not 90°. It is constant and somewhat less than 90° at all frequencies.

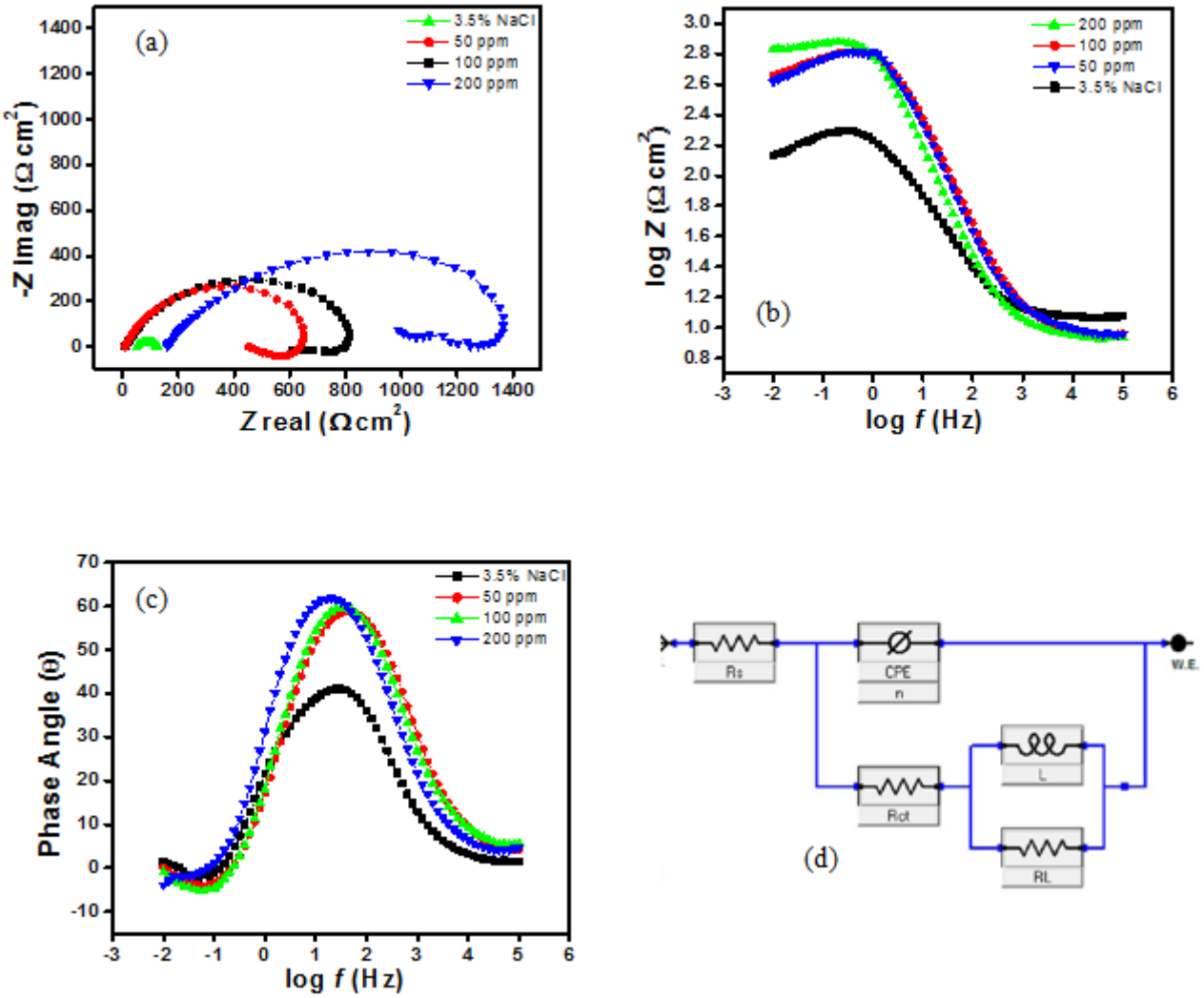

Figure 2. Electrochemical parameters (a) Nyquist plot (b) Bode plot (c) Theta frequency plot and (d) Equivalent circuit used.

The impedance parameters such as solution resistance (R_s), charge transfer resistance (R_{ct}), n, and inhibition efficiency (η%) are listed in Table 1. The values of η % are calculated using the following equation:

$$\eta(\%) = \frac{R_{ct,i} - R_{ct,0}}{R_{ct,i}} \times 100 \quad (2)$$

where, $R_{ct,i}$ and $R_{ct,0}$ are charge transfer resistances in presence and absence of inhibitor, respectively. It is clear from Table 1 that by increasing the inhibitor concentration the inhibition efficiency increases. This situation was the result of an increase in the surface coverage by the inhibitor, which led to an increase in the inhibition efficiency. Also any significant change in the values of the phase shift, *n*, was not observed in the absence and in the presence of T4PP. To predict the dissolution mechanism, the value of *n* can be used as an indicator [13]. The values of *n*, ranging between 0.616 and 0.864, indicate that the charge transfer process controls the dissolution mechanism of N80 steel in 3.5% NaCl solution saturated with CO_2 in the absence and in the presence of T4PP.

Table 2. EIS data for N80 steel in 3.5 wt. % NaCl at different concentrations of T4PP

Solution	R_s	R_{ct}	*n*	$Y_\circ$	*L*	η	Surf. coverage
	(Ω cm^2)	(Ω cm^2)		(Ω^{-1}s^n/cm^2)	(H cm^2)	%	θ
3.5% NaCl	10.0	121	.616	129	33	-	-
Inh 50 ppm	1.9	412	.722	105	22	70	.70
Inh 100 ppm	1.3	743	.827	91	19	83	.83
Inh 200 ppm	55.7	1356	.864	99	24	91	.91

It is apparent from Nyquist plots that the impedance response of N80 steel in inhibited 3.5% NaCl solution has changed significantly after the addition of T4PP to the solution. The Nyquist plots showed that on increasing T4PP concentration, charge transfer resistance increases from 121 Ω cm^2 for 3.5% NaCl solution saturated with CO_2 to 1356 Ω cm^2 for 200 ppm concentration of T4PP. From Table 1, it is clear that the greatest inhibition efficiency effect of 91% was observed at 200 ppm concentration of T4PP.

3.1.2. Polarization Measurements

Polarization curves for N80 steel at various concentration of T4PP in 3.5% NaCl solution saturated with CO_2 are shown in Figure 3. The extrapolation of Tafel straight line allows the calculation of the corrosion current density (I_{corr}). The values of I_{corr}, the corrosion potential (E_{corr}), cathodic and anodic Tafel slopes (b_c, b_a) and inhibition efficiency (η%) are given in Table 2. The (η%) is calculated using the following equation:

$$\eta\% = \left(\frac{I^0_{corr} - I^i_{corr}}{I^0_{corr}}\right) \times 100 \quad (3)$$

where I^0_{corr} and I^i_{corr} are the corrosion current density values without and with inhibitor, respectively.

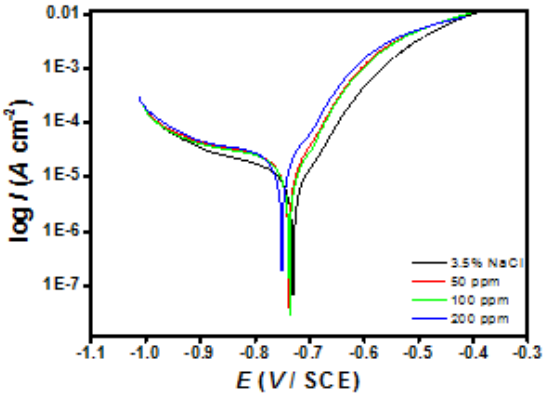

Figure 3. Tafel Polarization curves for N80 steel in 3.5% NaCl at a scan rate of 1 mV/s in the absence and presence of T4PP.

The change in b_a and b_c values as shown in Table 2 indicates that adsorption of T4PP modify the mechanism of anodic dissolution as well as cathodic hydrogen evolution [14]. The value of I_{corr} decreases with increasing T4PP concentration from 06.77 mA cm^{-2} for 3.5% NaCl solution to 74.96 µA cm^{-2} for 200 ppm concentration of inhibitor. From Figure 3, it is clear that both the cathodic and anodic reactions are inhibited and the inhibition increases as the inhibitor concentration increases in 3.5% NaCl solution, but the cathode is more polarized. From Table 2, it is clear that there was no definite trend in the shift of E_{corr} values, in the presence of various concentration of T4PP in 3.5% NaCl solution. This result indicated that T4PP can be classified as mixed type of inhibitor in 3.5% NaCl solution.

Table 2. Tafel data for N80 steel in 3.5 wt. % NaCl at different concentrations of T4PP

Solution	Concentration (ppm)	$-E_{corr}$ (mVvs.SCE)	I_{corr} (μAcm^{-2})	b_a (mVd^{-1})	b_c (mVd^{-1})	η (%)	θ
3.5%NaCl	-	730	06.77	69	214	-	-
T4PP	50	738	13.13	67	285	48	.48
T4PP	100	737	02	68	319	80	.80
T4PP	200	750	74.96	69	282	91	.91

3.3. Adsorption Isotherm

The adsorption of an organic adsorbate on to metal-solution interface can be represented by a substitutional adsorption process between the organic molecules in the aqueous solution phase ($Org_{(sol)}$) and the water molecules on the metallic surface ($H_2O_{(ads)}$) [15].

$$Org_{(sol)} + xH_2O \rightarrow Org_{(ads)} + xH_2O_{(sol)} \quad (4)$$

where, x is the size ratio representing the number of water molecules replaced by one molecule of organic adsorbate. Basic information on the interaction between the inhibitor and the N80 steel surface can be provided by the adsorption isotherm. For this purpose, the values of surface coverage (θ) at different concentrations (C) of T4PP in 3.5% NaCl solution saturated with CO_2 have been used to explain the best isotherm to determine the adsorption process. The values of θ can be easily determined from the ratio (η%) /100, where (η%) was obtained from electrochemical measurements. The correlation coefficients (R^2) were used to determine the best fit. Langmuir adsorption isotherm was used to plot the graph using the following equation:

$$\theta = \frac{K_{ads}C_{inh}}{1+K_{ads}C_{inh}} \quad \text{(Langmuir isotherm)} \quad (5)$$

where, K_{ads} is the equilibrium constant for the adsorption/desorption process. This equation can be rearranged to:

$$\frac{C_{inh}}{\theta} = \frac{1}{K_{ads}} + C_{inh} \quad (6)$$

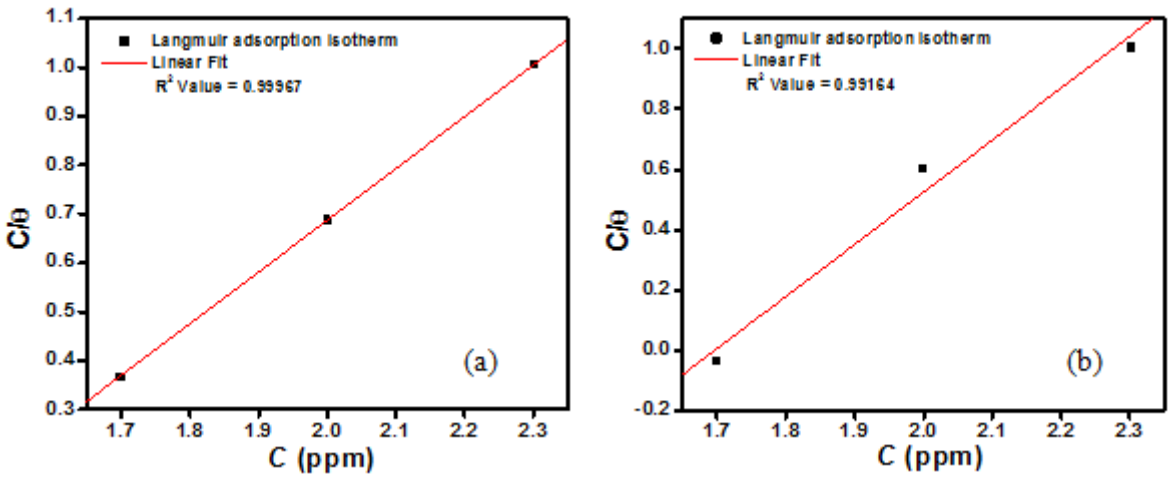

Figure 4. The Langmuir adsorption isotherm plots for N80 steel at different concentrations of T4PP by (a) EIS and (b) Tafel method.

By plotting values of C_{inh}/θ versus values of C_{inh}, straight line graphs were obtained (Fig. 4a, b), which suggested the adsorption of T4PP on metal surface obeyed Langmuir adsorption isotherm.where, a the molecular interaction parameter, θ is the surface coverage, C is the inhibitor concentration in equation (5). The obtained plots of the T4PP were almost linear with correlation coefficient (R^2) ranging 0.99967 for EIS (Figure 4a), 0.99164 for Tafel polarization (Figure 4b).

3.4. Scanning Electrochemical Microscopy (SECM)

Scanning electrochemical microscope (SECM) is a very useful technique for characterizing local electrochemical activity and pitting at films. The important advantage of the SECM technique is

that it operates on both insulating (coated / films) and conducting (non-coated) surfaces, thus allowing one to easily distinguish between the coated and corroded surfaces. Figure 5a, b presents the morphology of the specimens visualized by scanning electrochemical microscope. Prior to each SECM scanning experiment; the tip-sample distance was established by approach curves performed above the insulating part of the coating at -0.70 V. The status of a corroded sample was studied by monitoring the probe (tip potential: 0.5 V *vs* Ag/AgCl/saturated KCl reference electrode) and the substrate (tip potential: -0.7 V) in test solutions.

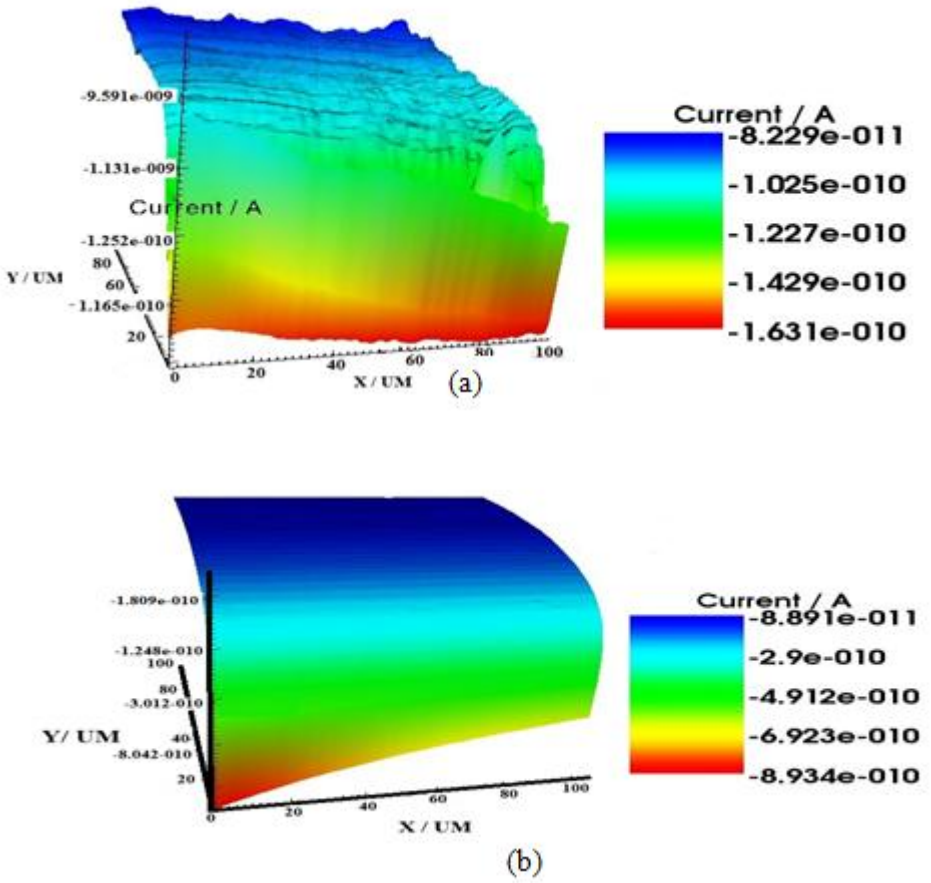

Figure 5. SECM imaging of (a) 3.5% NaCl solution and (b) 200 ppm T4PP at x-axis

When an insulating surface (having film or coating) as we used T4PP with 3.5% NaCl solution is approached in an SECM measurement the diffusion field surrounding the tip is hindered and the tip current decreases as shown in Figure 5b. This is typical for an insulating surface. On the contrary, an increase in the current is observed when a conductor i.e. blank 3.5% NaCl solution without T4PP is approached, because the redox mediator is regenerated at the surface. In the absence of T4PP the N80 steel surface remains conductive, which are evidenced by an increase in current as the surface is approached. Comparing the currents across the corroded sample and the specimens incorporated with inhibitor solution, the protection effect of the inhibitor can be justified.

3.5. Quantum Chemical Calculations

The structure and electronic parameters were obtained by means of theoretical calculations using the computational methodologies of quantum chemistry. The optimized molecular structures and frontier molecular orbital density distribution of the studied molecule are shown in Figure 6. The calculated quantum chemical parameters such as E_{HOMO}, E_{LUMO}, $\Delta E_{LUMO-HOMO}$, dipole moments (μ) are listed in Table 3. The molecular structure of T4PP shows that the molecules seems to adsorb on N80 steel surface by sharing of electrons of the nitrogen atoms with iron to form coordinated bonds and π-electron interactions of the aromatic rings.

Table 4. Calculated quantum chemical parameters of T4PP.

Quantum Parameters	T4PP
HOMO (hartree)	-0.20003
LUMO (hartree)	0.08415
ΔELUMO-HOMO (hartree)	0.28418
Dipole Moment (μ)	2.9843

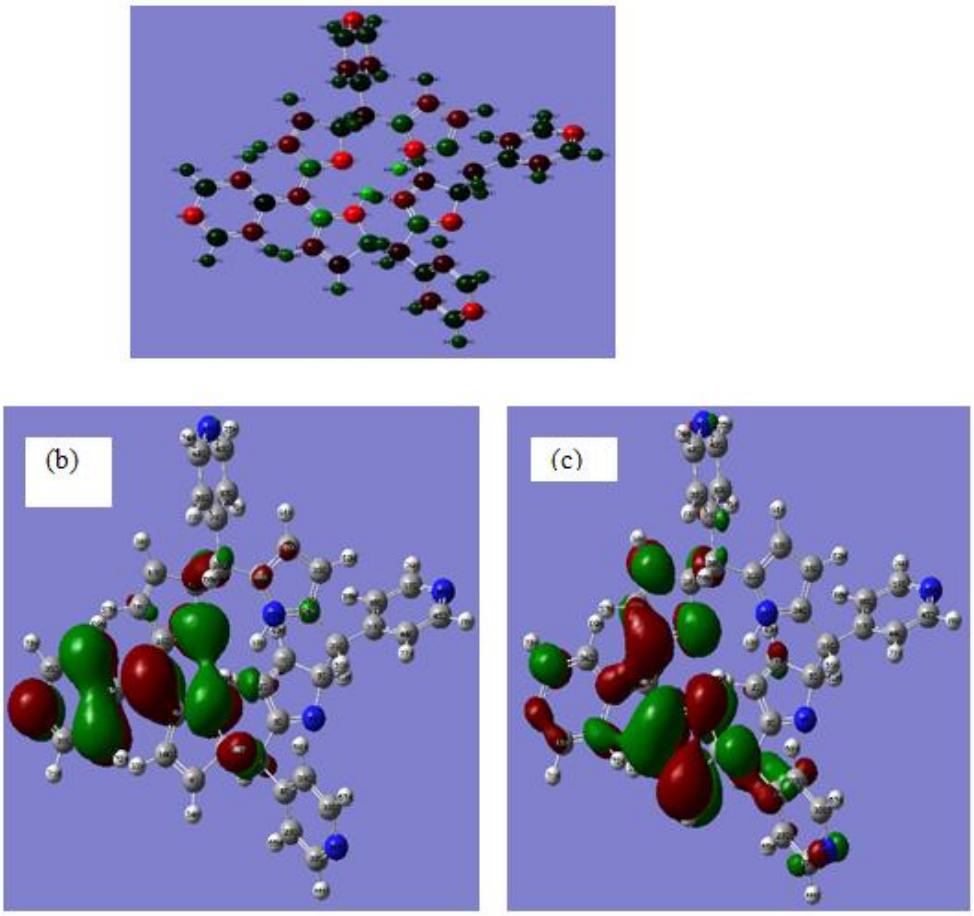

Figure 6. (a) Optimized molecular structure (b) HOMO and (c) LUMO molecular orbital density distribution of T4PP.

The value of highest occupied molecular orbital, E_{HOMO} indicates the tendency of the molecule to donate electrons to acceptor molecule with empty and low energy orbital. Therefore, the energy of the lowest unoccupied molecular orbital, E_{LUMO} indicates the tendency of the molecule to accept electrons [16]. The energy gap ΔE is an important parameter which is related to reactivity of the inhibitor molecule towards the metal surface. The interaction of inhibitor molecule to the metal surface is related to transfer of electrons from inhibitor to metal surface.

4. MECHANISM OF INHIBITION

The adsorption of the active constituents of T4PP on N80 steel surface reduces the surface area that is available for the attack of the aggressive ion from the 3.5% NaCl solution. It is not possible to consider a single adsorption mode between inhibitor and metal surface because of the complex nature of adsorption and inhibition of a given inhibitor [17, 18]. The adsorption of the T4PP can be attributed to the presence of N atoms and aromatic/heterocyclic rings in its chemical structure and also to the nitrogen-iron metal complex formation. Therefore, the possible reaction centres are unshared electron pair of hetero-atoms and π- electrons of aromatic/heterocyclic ring [19, 20]. The high performance of T4PP could also be due to large size of the molecule in the T4PP that covers wide areas on the metal surface and thus retarding the corrosion.

5. CONCLUSIONS

In this study, corrosion inhibition efficiency of 5,10,15,20-Tetra(4-pyridyl)-21H,23H-porphine on N80 steel in 3.5% NaCl was determined by electrochemical analysis. Electrochemical impedance spectroscopy data reveals increase in R_{ct} values, which accounted for good inhibition efficiency. The quantum studies confirmed the blockage of metal surface through adsorption process. All these data support good inhibition tendency of 5,10,15,20-Tetra(4-pyridyl)-21H,23H-porphine.

References

1. B. Obot, N. O. Obi-Egbedi, S. A. Umoren, E. E. Ebenso, *Int. J. Electrochem. Sci.* 5 (2010) 994-1007.
2. A. Y. El-Etre, *Corros. Sci.* 45 (2003) 2485-2495.
3. P. M. Krishnegoweda, V. T. Venkatesha, P. K. M. Krishnegoweda, S. B. Sivayogiraju, *Ind. Eng. Chem. Res.* 52 (2013) 722-728.
4. D. K. Yadav, D. S. Chauhan, I. Ahamad, M. A. Quraishi, *RSC Adv.* 3 (2013) 632-646.
5. S. Deng, X. Li, *Corros. Sci.* 55 (2012) 407-415.
6. G. Husnu, S. H. Ibrahim, *Ind. Eng. Chem. Res.* 51 (2012) 785-792.
7. G. Ji, S. K. Shukla, P. Dwivedi, S. Sundaram, R. Prakash, *Ind. Eng. Chem. Res.* 50 (2011) 11954-11959.
8. M. A. Chidiebere, C. E. Ogukwe, K. L. Oguzie, C N. Eneh, E. E. Oguzie, *Ind. Eng. Chem. Res.* 51 (2012) 668-677.
9. A. J. Bard, F. R. F. Fan, J. Kwak, O. Lev, *Anal. Chem.* 61 (1989) 132-138.

10. Gaussian 03, Revision E.01, M.J. Frisch, G.W. Trucks, H.B. Schlegel, G.E. Scuseria, M.A. Robb, J.R. Cheeseman, Jr. J.A. Montgomery, T. Vreven, K.N. Kudin, J.C. Burant, J.M. Millam, S.S. Iyengar, J. Tomasi, V. Barone, B. Mennucci, M. Cossi, G. Scalmani, N. Rega, G.A. Petersson, H. Nakatsuji, M. Hada, M. Ehara, K. Toyota, R. Fukuda, J. Hasegawa, M. Ishida, T. Nakajima, Y. Honda, O. Kitao, H. Nakai, M. Klene, X. Li, J.E. Knox, H.P. Hratchian, J.B. Cross, V. Bakken, C. Adamo, J. Jaramillo, R. Gomperts, R.E. Stratman, O. Yazyev, A.J. Austin, R. Cammi, C. Pomelli, J.W. Ochterski, P.Y. Ayala, K. Morokuma, G.A. Voth, P. Salvador, J.J. Dannenberg, V.G. Zakrzewski, S. Dapprich, A.D. Daniels, M.C. Strain, O. Farkas, D.K. Malick, A.D. Rabuck, K. Raghavachari, J.B. Foresman, J.V. Ortiz,Q. Cui, A.G. Baboul, S. Clifford, J. Cioslowski, B.B. Stefanov, G. Liu, Liashenko, A .P. Piskorz, I.Komaromi, R.L. Martin, D.J. Fox, T. Keith, M.A. Al-Laham, C.Y. Peng, A. Nanayakkara, M. Challacombe, P.M.W. Gill, B. Johnson, W. Chen, M.W. Wong, C. Gonzalez, J.A. Pople, Gaussian, Inc., Wallingford CT, (2007).
11. P. B. Raja, M. G. Sethuraman, *Mater. Lett.* 62 (2008) 2977-2979.
12. M. A. Quraishi, A. Singh, V. K. Singh, D. K. Yadav, A. K. Singh, *Mater. Chem. Phys.* 122 (2010) 114-122.
13. E. M. Sherif, *Int. J. Electrochem. Sci.* 6 (2011) 1479-1492.
14. A. Singh, E. E. Ebenso, M. A. Quraishi, *Int. J. Electrochem. Sci.* 7 (2012) 3409-3419.
15. A. Singh, I. Ahamad, M. A. Quraishi, *Arab. J. Chem.* (2013) http://dx.doi.org/10.1016/j.arabjc.2012.04.029.
16. I. Ahamad, R. Prasad, M. A. Quraishi, *J. Solid State Electrochem.* 14 (2010) 2095-2105.
17. K. F. Khaled, *Electrochim. Acta.* 54 (2009) 6523-6532.
18. A. Singh, I. Ahamad, V. K. Singh, M. A. Quraishi, *J. Solid State Electrochem.* 15 (2011) 1087-1097.
19. A. Khamis, M. M. Saleh, M. I. Awad, *Corros. Sci.* 66 (2013) 343-349.
20. P. B. Raja, A. K. Qureshi, A. A. Rahim, H. Osman, K. Awang, *Corros. Sci.* 69 (2013) 292-301.